BALKAN JOURNAL OF ELECTRICAL & COMPUTER ENGINEERING, Vol. 13, No. 2, June 2025
Research Article

Breast Cancer Detectability and Tumor Differentiation Based on Microwave Dielectric Property Changes with Reverse Time Migration

Cemanur Aydinalp and Gulsah Yildiz

***Abstract*—Breast cancer detection and treatment have advanced significantly with imaging technologies, but challenges remain in distinguishing the type and stage of tumors. Microwave imaging (MWI) offers a promising alternative due to its non-ionizing nature and its ability to exploit dielectric property (DP) contrast. This study investigates the effectiveness of MWI in detecting and characterizing tumors using a phantom for breast tissue and tumor-mimicking NaCl solutions with various DPs (0.1 M, 0.2 M, 0.4 M and 0.8 M). First, the Cole-Cole parameters of these materials were calculated using DP measurements obtained from the open-ended coaxial probe method in order to provide broadband frequency analysis. Furthermore, the developed MWI system was utilized to evaluate tumor detectability and differentiation based on these DP changes. The MWI experiment was performed with 12 Vivaldi antennas between 0.6-2.6 GHz, and the results were analyzed from two different positions. The results indicate that the MWI system can effectively distinguish tumors with different DPs from each other using quantitative differential imaging due to its sensitivity to variations. To this end, the inverse time migration (RTM) method was employed to compare reference-target pairs (RTP) to generate an image of a tissue-mimicking phantom with tumors. The results show a high correlation between RTP image contrast and the target-reference DP difference.**

Index Terms— **Dielectric property of tissue-mimicking materials, microwave imaging, breast cancer detection, open-ended coaxial probe, Cole-Cole parameters.**

I. Introduction

BREAST cancer is one of the most common cancers worldwide [1]–[3]. The complexity of breast tissue has made the detection, diagnosis and treatment of breast cancer the subject of extensive and long-term research [4]–[7]. These studies comprise the measurement of tumor dielectric properties and tissue classification [4], [5], accurate tumor localization [6], [7], tumor stage detection [8], [9] and tumor treatment [10], [11]. Accurate localization and differentiation of the tumor into carcinogenic stages are crucial for the patient's treatment process and early diagnosis is essential in the breast cancer treatment plan [12]. Diagnostic methods include mammography, ultrasound and magnetic resonance imaging (MRI). Mammography uses X-rays, a type of ionizing radiation, to detect tumors [8]. Although ultrasound and MRI do not emit harmful radiation, ultrasound provides low-resolution images and lacks consistency in archival quality due to differences in measurement positions by different practitioners [13]. In contrast, while MRI does not emit harmful waves, it is a costly option for early detection [14].

Microwave imaging (MWI) is an emerging technique with applications in medical imaging, earth observation and other fields [15]–[17]. MWI employs microwaves, a non-ionizing portion of the electromagnetic spectrum ranging from 0.3 to 30 GHz. This specific range provides the precise frequencies necessary to penetrate biological tissues and allows imaging at acceptable resolution without emitting high power levels into the body. MWI primarily utilizes the dielectric properties (DPs) contrast of materials to create images. Normal and abnormal tissues exhibit a wide range of DPs, which provide the contrast necessary for imaging [18]. This is particularly advantageous in dense breast tissue, where tumors have significantly different dielectric properties compared to healthy tissues. These differences increase the efficiency of MWI. In contrast, other imaging techniques are less sensitive in detecting differences between healthy and tumor regions in dense breast tissue [19].

Quantitative MWI techniques aim to provide an image where the contrast directly depends on the magnitude of physical parameters such as DPs. These methods are often iterative, computationally expensive, and time-consuming [20]. On the other hand, qualitative imaging techniques are faster and easier to implement, providing an indication of the magnitude correlation [21]. The linear sampling method (LSM) and the factorization method (FM) are the two most commonly used qualitative methods for MWI [21]. These methods have similar mathematical backgrounds and do not require prior knowledge. They can be formulated from the electric field [22] or scattering parameters [21], while the latter is more efficient to use directly from an experimental setup. Near- field orthogonality sampling method (NOSM), multiple signal classification (MUSIC) and reverse time migration (RTM) methods are some other qualitative methods used in MWI [23]–[25]. In [25], the electric field mathematical background for the RTM method is provided and extended to use the scattering parameters obtained from an experimental setup. A frequency range of 2-4 GHz with a step size of 0.1 GHz is used for single-slice imaging of a tissue-mimicking phantom. Furthermore, this approach is applied to detect breast cancer using differential imaging, which increases the contrast of the target region relative to the

Cemanur Aydinalp and **Gulsah Yildiz** are with the Department of Electronics and Communication Engineering, Faculty of Electrical and Electronics Engineering, Istanbul Technical University, Istanbul, 34469, TURKEY e-mail: aydinalp16@itu.edu.tr
Manuscript received Jul 30, 2024; accepted Jan 21, 2025.
DOI: 10.17694/bajece.1521841

background by using the breast pair as the reference and the target [26]. In addition, DL-enhanced RTM has the potential to improve computational efficiency and result accuracy in medical microwave imaging [27].

The Cole-Cole method, a mathematical model, is frequently used in the literature to represent dielectric behavior over a wide frequency range using a few parameters [28]. This model provides essential parameters to establish the DP of materials based on the operation frequency. Particle swarm optimization and the generalized Newton-Raphson methods are employed to determine the Cole-Cole parameters based on DP measurements. Therefore, it is crucial to accurately obtain the DP of tissue-mimicking phantoms based on the research to ensure precision in biomedical applications.

In this study, the dielectric properties of tumors were altered using breast tissue-mimicking phantom, and the detectability of these changes was analyzed using MWI methods. The main contributions of this study are:

- The MWI experimental setup and the MWI algorithm to identify the normal and abnormal tissue characteristics are demonstrated.
- A detailed analysis of how tumors with varying DPs can be differentiated from each other using the MWI algorithm is given.
- The correlation between DP differences and the corresponding MWI results is presented.
- The Cole-Cole parameters for the DPs of breast tissue-mimicking phantom and tumor materials are provided.

These contributions collectively offer the potential to distinguish the type or stage of a tumor rather than merely identifying the presence of a tumor. Furthermore, during treatment, the DP of the tumor can undergo changes, and the results demonstrate that the MWI system is capable of detecting these alterations. The remainder of this paper is organized as follows: Section 2 details the formulation and preparation of the tissue-mimicking phantom, the experimental setups for DP measurements, and the MWI system. Additionally, this section describes the extraction of Cole-Cole parameters from DP characterization. Section 3 presents the results regarding the sensitivity of the MWI system to variations in DPs. The sensitivity analysis is performed based on a comparison of DP measurements and MWI methods. Conclusions are drawn in Section 4.

II. MATERIAL AND METHOD

A. Tissue-Mimicking Phantom

Tissue-mimicking phantoms are employed in medical fields to develop and assess emerging devices before conducting animal experiments and clinical tests. Therefore, several studies in the literature have been carried out to simplify the preparation of the phantom and enhance its long-term usability [18], [29], [30]. In this study, a breast fat-mimicking phantom shown in Fig.1a was prepared using the formula obtained from [18]. The phantom preparation procedure was repeated twice to designate areas for the placement of NaCl solutions (0.1 M, 0.2 M, 0.4 M, and 0.8 M). To summarize the phantom preparation, the following steps were followed:

- 17 g (dry mass) of calfskin gelatin (obtained from Vyse Gelatin Company, Schiller Park, IL, USA) was added to 95 ml of distilled water. The key procedure to facilitate gelatin dissolution in water involves sprinkling the gelatin over the water to prevent clumping.
- A total of 400 ml of oil and the mixture of distilled water and gelatin were covered with plastic film and placed into a hot water jacket. The transition of the gelatin-water mixture to a transparent yellow color is a crucial part of this step.
- When the oil and mixture cooled down to 50°C, the oil was gradually added while stirring with a magnetic stirrer.
- Next, 0.56 ml of Fairy liquid surfactant (Procter and Gamble, Turkey) was introduced into the mixture while stirring. To prevent bubbling, the stirrer speed was reduced during the addition of the detergent.
- Then, a formaldehyde solution (1.08 g) was incorporated into the mixture.
- Finally, the liquid form of the phantom was poured into half of the breast model. After the first phantom solidified, a straw with a sealed bottom was placed over the solid phantom. A second liquid phantom, prepared using the same procedure, was poured into the remaining part of the breast model and allowed to solidify. The final breast phantom model consists of two layers, with an empty hole for the tumor in the second layer.

Note that the diameter and height of the breast phantom model are 12 cm and 14 cm, respectively. The diameter and length of the straw placed in the phantom to represent the tumor are 1 cm and 10 cm.

B. Experimental Setup

The experimental setup consists of the dielectric property measurement and the imaging systems. First, N5230A PNA Series Network Analyzer (Santa Clara, CA, USA) and Speag DAK 3.5-mm-diameter open-ended coaxial probe (Zurich, Switzerland) were utilized to measure the dielectric property of the breast phantom and four different NaCl solutions (0.1 M, 0.2 M, 0.4 M, and 0.8 M). The dielectric property measurement setup is displayed in Fig.1b. The frequency range of measurements was between 0.5-12 GHz with a resolution of 100 MHz, resulting in 116 frequency points.

Second, the imaging system is composed of 24 Vivaldi antennas connected to a 24-channel Rohde & Schwarz ZNBT8 network analyzer with RF cables (50Ω impedance). Two groups of 12 antennas were placed facing each other with a 14 cm gap in between, as in Fig.1c. Antennas were placed between wooden insulators to prevent coupling.

C. Dielectric Property Characterization

In this section, the results obtained from the dielectric property measurement setup are examined for use in the imaging system. The dielectric property (real -ε′- and imaginary -ε″- parts) of NaCl solutions and breast phantom is shown in Fig. 2 and 3, respectively. Furthermore, the dielectric properties of phantom and NaCl solutions at 0.6 and 2.6 GHz are listed in Table I. The Cole-Cole parameters are calculated to allow broadband frequency analysis. In addition, these parameters can

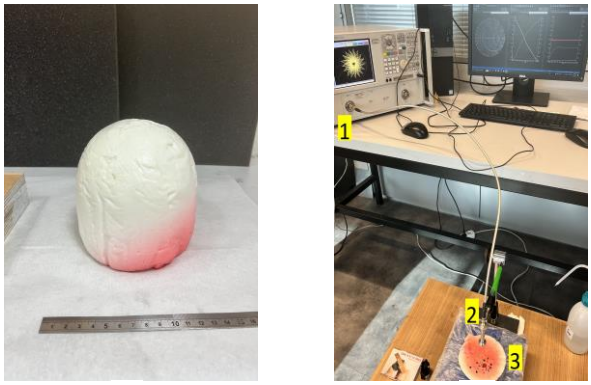

(a) (b)

(c)

Fig.1. Breast phantom and experimental setup consisted of two measurement systems. (a) Breast phantom (colored to indicate two layers). (b) Dielectric property measurement system 1. N5230A PNA Series Network Analyzer, 2. Speag DAK 3.5-mm-diameter probe, 3. phantom. (c) Imaging system 1. 24-channel Rohde & Schwarz ZNBT8 Network Analyzer, 2. Rohde & Schwarz ZN-Z154 calibration kit, 3. two sets of 12 antennas and 4. phantom.

be used in imaging systems with different frequency ranges without dielectric property measurements. To this end, the generalized Newton-Raphson method, an iterative method for solving nonlinear least squares problems, is used to calculate parameters of the one-pole Cole-Cole model [31], [32]:

$$\varepsilon(\omega) = \varepsilon_\infty + \frac{(\varepsilon_s - \varepsilon_\infty)}{1 + (i\omega\tau)^{1-\alpha}} \quad (1)$$

$\varepsilon(\omega)$ is the complex dielectric permittivity as a function of angular frequency (ω). ε_∞ and ε_s represent the high-frequency permittivity and the static (or DC) permittivity, respectively. τ stands for the relaxation time. α is the Cole-Cole parameter, typically between 0 and 1. Generalized Newton Raphson calculates the Cole-Cole parameters using the Euclidean Distance to evaluate the error rate between the calculated and measured dielectric properties, and the corresponding error calculation is given below:

$$e = \frac{1}{N}\sum_{i=1}^{N}\left[\left(\frac{\varepsilon'_{\omega_i} - \hat{\varepsilon}'_{\omega_i}}{median\left[\varepsilon'_{\omega_i}\right]}\right) + \left(\frac{\varepsilon''_{\omega_i} - \hat{\varepsilon}''_{\omega_i}}{median\left[\varepsilon''_{\omega_i}\right]}\right)\right]^2 \quad (2)$$

ε' and ε'' are the real and imaginary parts of the measured dielectric property. $\hat{\varepsilon}'_{\omega_i}$ and $\hat{\varepsilon}''_{\omega_i}$ represent the real and imaginary parts of the data fitted to the Cole-Cole model. N is the number of frequency points. The algorithms continued to run until the error rate was below a threshold value of 0.001. The obtained Cole-Cole parameters of phantom and NaCl solutions are presented in Table II.

TABLE I
THE DIELECTRIC PROPERTY OF BREAST PHANTOM AND NACL SOLUTIONS AT 0.6 AND 2.6 GHz.

Samples	ε'		ε''	
	0.6 GHz	2.6 GHz	0.6 GHz	2.6 GHz
Phantom	8.22	7.45	1.37	1.39
0.1 M	77.88	75.31	37.18	17.79
0.2 M	77.09	73.53	71.98	25.90
0.4 M	73.53	70.56	133.20	39.35
0.8 M	68.91	64.82	248.90	64.82

TABLE II
THE COLE-COLE PARAMETERS OF THE SAMPLES: BREAST PHANTOM AND NACL SOLUTIONS WITH FOUR DIFFERENT MIXTURES.

Samples	Cole-Cole Parameters					Error (10^{-4})
	ε_s	ε_∞	τ (ps)	α	σ (S/m)	
Phantom	8.38	2.62	12.90	0.2710	0.028	9.33
0.1 M	77.03	9.45	8.9	0.0281	1.17	8.02
0.2 M	75.92	11.60	9.48	0.0473	2.35	8.91
0.4 M	73.04	6.04	8.13	0.0697	4.40	6.02
0.8 M	67.72	2.56	7.14	0.1257	8.19	6.37

D. *Imaging System Protocol*

In the imaging system, a three-stage protocol was implemented to detect tumor location. First, the 24 cables connected to VNA were calibrated at 0.6-2.6 GHz using Rohde & Schwarz ZN-Z154 calibration kit. Thus, the reference plane was shifted from the network analyzer to the cable tip. Then, the cables are connected to the antennas. Note that the antennas are secured in a fixed position to prevent the bending of rigid RF cables. The phantom was then placed between the two antenna arrays. A dock (shown in Fig. 1c as white holder) was used to rotate the phantom from its center, with the tumor position closest to the fifth and ninth antennas throughout the experiments. Second, the measurements were initiated when the tumor location was not filled with NaCl solutions. After, NaCl solutions (0.1 M, 0.2 M, 0.4 M and 0.8 M) were sequentially injected into the empty tumor location with a syringe, 10 ml at a time, and the tumor location was drained before each injection. Thus, the measurement capabilities of the antennas were investigated for tumors with four different dielectric properties at two different locations in the imaging system. For the imaging results, a differential MWI approach was applied in which reference and target measurements were taken successively to detect the target tumor [7], [26]. The Inverse Time Migration (RTM) method was used as the imaging algorithm, and the inputs for the algorithm were the reflection and transmission coefficients obtained from the antennas [25]. Note that since the RTM method uses the absolute value of the difference of the scattering parameters,

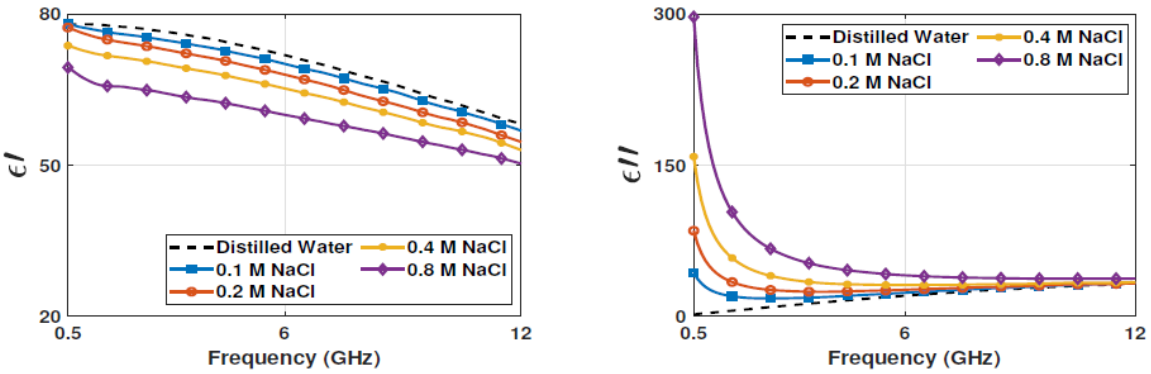

Fig. 2. Dielectric property of distilled water and NaCl solutions (0.1 M, 0.2 M, 0.4 M, and 0.8 M). (a) Real part and (b) imaginary of the dielectric properties at 0.5-12 GHz.

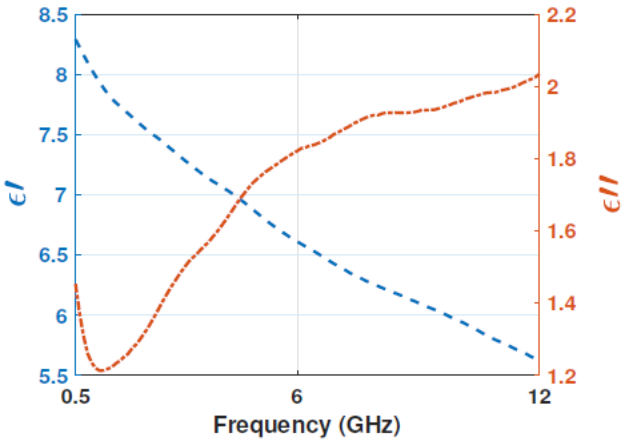

Fig. 3. Dielectric property (real part and imaginary) of breast phantom at 0.5 - 12 GHz.

the reference and target solutions can be used interchangeably. However, we will use these terms to facilitate clarity.

III. RESULTS

In this work, the sensitivity of the MWI system to changes in dielectric properties was investigated. To this end, four different NaCl solutions (0.1 M, 0.2 M, 0.4 M, and 0.8 M) were injected into the empty tumor location of the phantom. The percentage differences (PD) of the dielectric properties for the injected target NaCl solution with respect to the reference measurement at 0.6 and 2.6 GHz frequencies were calculated by the following equation:

$$PD = \left| \frac{Target\ Value - Reference\ \ Value}{Reference\ Value} \right| \times 100\%$$

The percentage differences of the dielectric properties are listed in Table III. For 0.6 GHz, in the case of 0.1 M reference solution, the percentage differences of 0.2 M, 0.4 M, and 0.8 M are 33, 63.28, and 82.05, respectively. When the reference solution was 0.2 M, the difference values 40.38 for 0.4 M and 68.58 for 0.8 M were calculated. Between 0.4 M reference and 0.8 M target solutions, the difference equals 44.83. In the case of distilled water (DW) reference solution, the percentage differences of 0.1 M, 0.2 M, 0.4 M, and 0.8 M are 41.17, 66.69, 86.65, and 95.80, respectively. The corresponding difference values for 2.6 GHz are provided in the second row of Table III. Therefore, the percentage differences derived from the data collected at 0.6 GHz and 2.6 GHz indicate that the highest differences occur at 0.6 GHz. This trend suggests that lower frequencies are more effective for tumor differentiation.

The results, the images of reference-target pairs (RTP), shown in Fig. 4 and Fig. 5, are obtained from the qualitative differential MWI algorithm using reference-target pairs suggested in Table III. For example, to analyze the results (in Fig. 4a) for the 0.1 M-0.2 M difference, an experiment was performed for the fifth antenna position. First, the scattering parameters were collected when the tumor region was filled with the reference 0.1 M NaCl solution and the tumor was positioned as close to the fifth antenna as possible using the dock. Then, the region was drained, and the second set of measurements was collected when the tumor region was filled with 0.2 M NaCl solution. The collected scattering parameters were subtracted from each other as the differential imaging suggests, and the final image was retrieved by the RTM method, as displayed in Fig. 4a. The highest value of the image, which is 0.049, is close to the fifth antenna, as expected, in accordance with the tumor position. Keeping the reference as 0.1 M, two more measurements were collected when the tumor region was filled with 0.4 M and 0.8 M NaCl solutions, and the highest values of the retrieved images are at the same position as the first image (Fig. 4b and Fig. 4c). However, the highest values are 0.103 for 0.1 M-0.4 M image of RTP and 0.144 for 0.1 M-0.8 M image of RTP. For Fig. 4a-4c, the increase of the highest value in the images is in good agreement with the increase of the difference values for the two different frequency points given in Table III. Changing the reference solution to 0.2 M, two measurements were performed for targets 0.4 M and 0.8 M solutions, and the highest values of the resulting images of RTP are 0.058 and 0.115, respectively, as illustrated in Figs. 4d and 4e. Fig. 4f shows the image of RTP for 0.4 M-0.8 M pair with 0.063 as the highest value. For all the images in Fig. 4, the highest value positions indicate the tumor positions.

 ISSN: 2147-284X http://dergipark.gov.tr/bajece

TABLE II
THE PERCENTAGE DIFFERENCES OF THE DIELECTRIC PROPERTIES FOR REFERENCE AND TARGET SOLUTIONS AT 0.6 AND 2.6 GHz.

Samples		0.1-0.2 M	0.1-0.4 M	0.1-0.8 M	0.2-0.4 M	0.2-0.8 M	0.4-0.8 M	DW-0.1 M	DW-0.2 M	DW-0.4 M	DW-0.8 M
PD (%)	0.6 GHz	33	63.28	82.05	40.38	68.58	44.83	41.17	66.69	86.65	95.80
	2.6 GHz	10.65	27.33	52.56	17.05	43.51	28.48	10.87	21.44	37.73	61.74

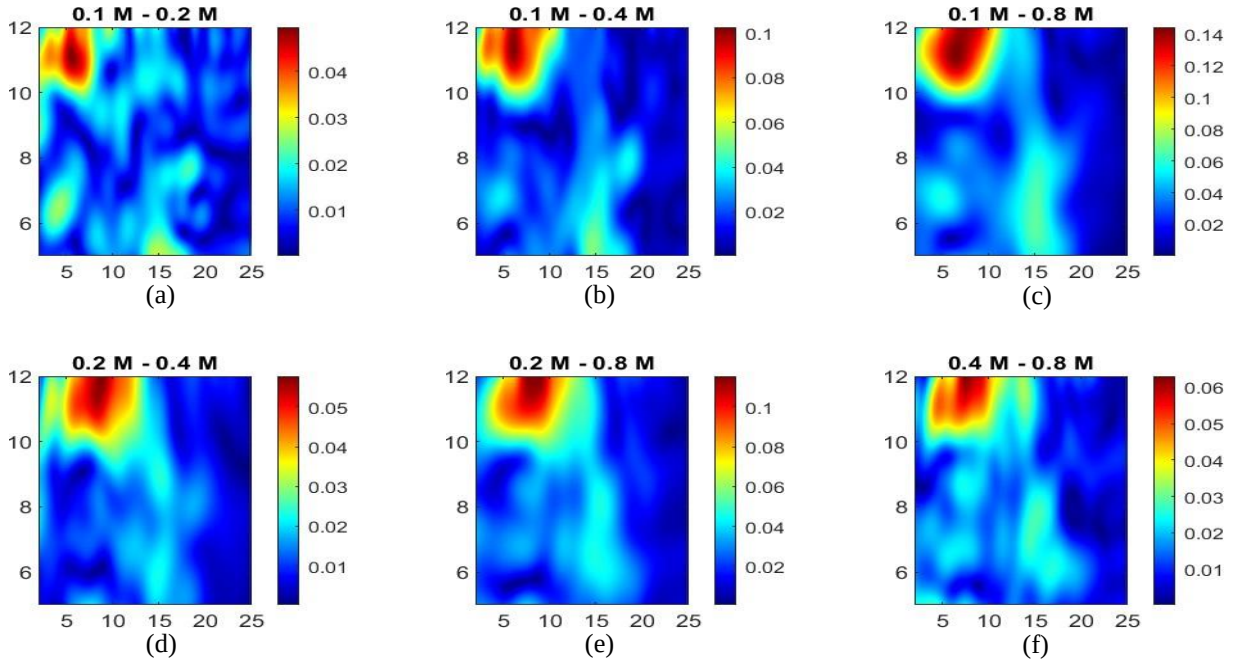

Fig. 4. Qualitative differential microwave imaging (MWI) results when the tumor is positioned near the fifth antenna. The reference-target pairs (RTP) are as follows: (a-c) 0.1 M solution against 0.2 M, 0.4 M, and 0.8 M, respectively; (d-e) 0.2 M solution as the reference for 0.4 M and 0.8 M targets; (f) 0.4 M solution as the reference for 0.8 M target.

Fig. 5 shows the images of RTP when the tumor region was positioned as close to the ninth antenna as possible. The highest values of the images are all at the same position, indicating the position of the tumor region. When the reference solution was 0.1 M, the highest values of the RTP images were 0.051, 0.111, and 0.158 for the targets 0.2 M, 0.4 M, and 0.8 M, respectively. Moreover, when 0.2 M is the reference, the highest values of the RTP images for 0.4 M and 0.8 M targets are 0.061 and 0.118, respectively. Last, the 0.4 M - 0.8 M RTP image has the highest value of 0.053. Note that the highest values obtained for the same reference-target pairs are comparable when the tumor position is in the fifth and ninth positions. Finally, distilled water was utilized as reference, and four NaCl solutions were measured as targets (Fig. 5g, 5h, 5i and 5j). Since the dielectric properties between distilled water and the targets exhibit significant differences, the corresponding highest values (0.88, 0.138, 0.199, and 0.245) are higher than those of the other pairs.

IV. CONCLUSION

Breast cancer remains one of the most prevalent cancers worldwide, driving comprehensive research into its detection, diagnosis, and treatment, including the dielectric properties measurement of tumors, tissue classification, accurate tumor localization, staging of tumors, and the development of treatment strategies. This study aims to investigate whether the MWI system can distinguish differences in the DPs of tumor tissues. To this end, a phantom was prepared to mimic healthy breast tissue, and four different NaCl solutions (0.1 M, 0.2 M, 0.4 M, and 0.8 M) were utilized to represent tumors producing variation in DPs. The DPs of the phantom and NaCl solutions were measured with an open-ended coaxial probe, and the Cole-Cole parameters were retrieved from these measurements using the generalized Newton-Raphson method. Furthermore, the MWI system was utilized to collect data using 12 Vivaldi antennas operating between 0.6 and 2.6 GHz from a sample containing both healthy and tumor-mimicking materials. These data were used in the RTM imaging algorithm to demonstrate that MWI can accurately detect and differentiate tumors with different DPs. The results are analyzed for two different positions: close to the fifth and ninth antennas. As the DPs discrepancy between tumors increases, the RTP image shows higher values due to the characteristics of the imaging algorithm representing tumor location based on reference and target pairs. For instance, with a 0.1 M reference solution, the RTP images produced the highest values of 0.051, 0.111, and 0.158 for targets of 0.2 M, 0.4 M, and 0.8 M, respectively. Additionally, the ability of the MWI system to detect the changes in DPs would be an essential tool for monitoring the temperature-dependent DPs during the heat treatment processes. Therefore, the results highlight that the MWI system not only detects the presence of tumors but also distinguishes their type and stage

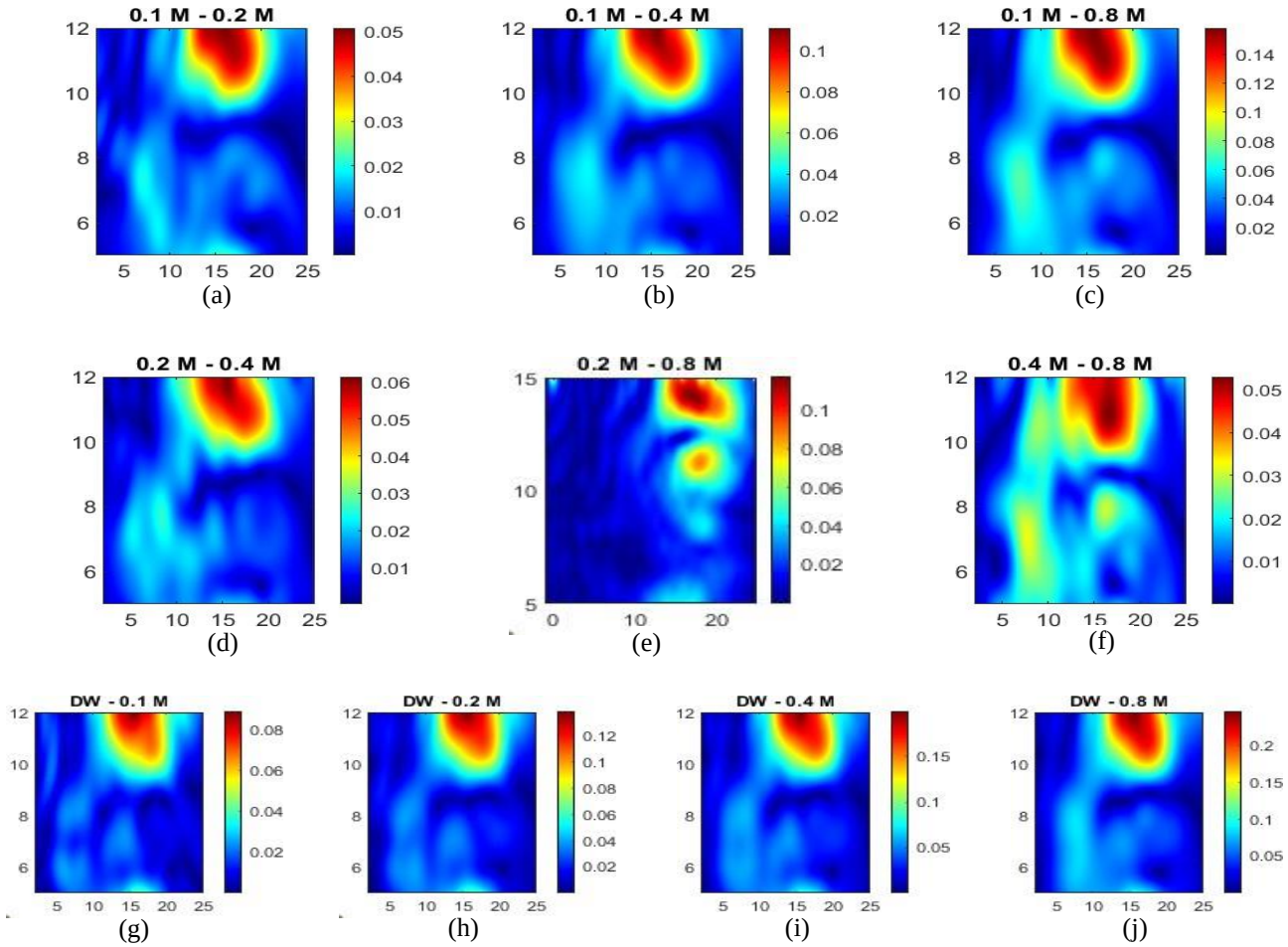

Fig. 5. Qualitative differential MWI results when the tumor is positioned near the ninth antenna. The RTP images are as follows: (a-c) 0.1 M solution against 0.2 M, 0.4 M, and 0.8 M, respectively; (d-e) 0.2 M solution as the reference for 0.4 M and 0.8 M targets; (f) 0.4 M solution as the reference for 0.8 M target; (g-j) distilled water (DW) as the reference for 0.1 M, 0.2 M, 0.4 M, and 0.8 M targets, respectively.

based on changes in DPs. Apart from these, providing Cole-Cole parameters in this study enhances both the reproducibility and sensitivity of MWI in biomedical applications. To conclude, MWI systems are a promising, non-invasive, and cost-effective method for breast cancer detection and monitoring. In future work, further adjustment is required to be implemented to utilize in clinical environment. To this end, extensive datasets can be generated to enable the training, validation, and testing of DL models in conjunction with the RTM algorithm. Therefore, with these advancements, MWI systems could significantly contribute to early diagnosis and more effective treatment strategies for breast cancer. Although numerous studies have been conducted on tumor detection, the importance of distinguishing between different tumor types has often been overlooked. This study emphasizes the significance of recognizing variations among tumor conditions, highlighting the need for accurate differentiation in medical imaging for improved diagnosis and treatment. However, several limitations should be noted. Firstly, the experiments were conducted using phantoms, which, although useful for simulating tumor conditions, do not fully replicate the complexity of human tissues. Clinical validation is essential to confirm the results and refine the system's performance in real-world applications. Additionally, the study focused on a limited frequency range (0.6-2.6 GHz), and further investigation into the effect of different frequencies and more diverse tissue models could enhance the system's accuracy. Continued advancements in this technology could significantly improve early diagnosis and treatment.

ACKNOWLEDGMENT

The authors are with the Laboratory for Medical Device Research, Development and Application, Istanbul Technical University, Istanbul, 34469, TURKEY. Furthermore, this study was supported by the Research Fund of the Istanbul Technical University Project Number MAB-2024-45450 and by the Scientific and Technological Research Council of Turkey (TUBITAK) under Grant Number 123N484. The authors thank TUBITAK for their support.

REFERENCES

[1] A. E. Giuliano, R. C. Jones, M. Brennan, and R. Statman, "Sentinel lymphadenectomy in breast cancer." Journal of Clinical Oncology, vol. 15, no. 6, pp. 2345–2350, 1997.

[2] H. Sung, J. Ferlay, R. L. Siegel, M. Laversanne, I. Soerjomataram, A. Jemal, and F. Bray, "Global cancer statistics 2020: Globocan estimates of incidence and mortality worldwide for 36 cancers in 185 countries," CA: a cancer journal for clinicians, vol. 71, no. 3, pp. 209–249, 2021.

[3] R. L. Siegel, N. S. Wagle, A. Cercek, R. A. Smith, and A. Jemal, "Colorectal cancer statistics, 2023," CA: a cancer journal for clinicians, vol. 73, no. 3, pp. 233–254, 2023.
[4] C. Ss, R. K. Mishra, A. Swarup, and T. Jm, "Dielectric properties of normal & malignant human breast tissues at radiowave & microwave frequencies." Indian journal of biochemistry & biophysics, vol. 21 1, pp. 76–9, 1984. [Online]. Available: https://api.semanticscholar.org/CorpusID:35827569
[5] E. Onemli, S. Joof, C. Aydinalp, N. Pastacı Özsobacı, F. Ates¸ Alkan, N. Kepil, I. Rekik, I. Akduman, and T. Yilmaz, "Classification of rat mammary carcinoma with large scale in vivo microwave measurements," Scientific reports, vol. 12, no. 1, p. 349, 2022.
[6] P. C. Gøtzsche and K. J. Jørgensen, "Screening for breast cancer with mammography," Cochrane database of systematic reviews, no. 6, 2013.
[7] A. Janjic, M. Cayoren, I. Akduman, T. Yilmaz, E. Onemli, O. Bugdayci, and M. E. Aribal, "Safe: A novel microwave imaging system design for breast cancer screening and early detection—clinical evaluation," Diagnostics, vol. 11, no. 3, p. 533, 2021.
[8] J. C. Lashof, I. C. Henderson, and S. J. Nass, "Mammography and beyond: developing technologies for the early detection of breast cancer," 2001.
[9] J. N. Wolfe, "Breast patterns as an index of risk for developing breast cancer," American Journal of Roentgenology, vol. 126, no. 6, pp. 1130–1137, 1976.
[10] N. I. of Health Consensus Development Panel et al., "Special report. treatment of primary breast cancer," N Engl J Med, vol. 301, p. 340, 1979.
[11] G. Yildiz, H. Yasar, I. E. Uslu, Y. Demirel, M. N. Akinci, T. Yilmaz, and I. Akduman, "Antenna excitation optimization with deep learning for microwave breast cancer hyperthermia," Sensors, vol. 22, no. 17, p. 6343, 2022.
[12] I. Barco, C. Chabrera, M. G. Font, N. Gimenez, M. Fraile, J. M. Lain, M. Piqueras, M. C. Vidal, M. Torras, S. Gonza´lez et al., "Comparison of screened and nonscreened breast cancer patients in relation to age: a 2-institution study," Clinical Breast Cancer, vol. 15, no. 6, pp. 482–489, 2015.
[13] B. Ranger, P. J. Littrup, N. Duric, P. Chandiwala-Mody, C. Li, S. Schmidt, and J. Lupinacci, "Breast ultrasound tomography versus MRI for clinical display of anatomy and tumor rendering: preliminary results," American Journal of Roentgenology, vol. 198, no. 1, pp. 233–239, 2012.
[14] E. Aslan and Y. Ozupak, "Comparison of machine learning algorithms for automatic prediction of Alzheimer's disease," *Journal of the Chinese Medical Association*, pp. 10–1097, 2024.
[15] S. Dey and A. O. Asok, "A review on microwave imaging for breast cancer detection," in *2024 IEEE Wireless Antenna and Microwave Symposium (WAMS)*, 2024, pp. 1–5.
[16] S. Di Meo, A. Cannata`, C. Blanco-Angulo, G. Matrone, A. Martinez-Lozano, J. Arias-Rodriguez, J. M. Sabater-Navarro, R. Gutierrez-Mazon, H. Garcia-Martinez, E. Avila-Navarro *et al.*, "Multi-layer tissue-mimicking breast phantoms for microwave-based imaging systems," *IEEE Journal of Electromagnetics, RF and Microwaves in Medicine and Biology*, 2024.
[17] D. Bhargava, P. Rattanadecho, and K. Jiamjiroch, "Microwave imaging for breast cancer detection-a comprehensive review," *Engineered Science*, vol. 30, p. 1116, 2024.
[18] M. Lazebnik, E. L. Madsen, G. R. Frank, and S. C. Hagness, "Tissue-mimicking phantom materials for narrowband and ultrawideband microwave applications," *Physics in Medicine & Biology*, vol. 50, no. 18, p. 4245, 2005.
[19] P. E. Freer, "Mammographic breast density: impact on breast cancer risk and implications for screening," *Radiographics*, vol. 35, no. 2, pp. 302–315, 2015.
[20] A. Yago Ruiz, M. Cavagnaro, and L. Crocco, "An effective framework for deep-learning-enhanced quantitative microwave imaging and its potential for medical applications," *Sensors*, vol. 23, no. 2, p. 643, 2023.
[21] M. N. Akinci, T. Caglayan, S. Ozgur, U. Alkasi, H. Ahmadzay, M. Abbak, M. Cayoren, and I. Akduman, "Qualitative microwave imaging with scattering parameters measurements," *IEEE Transactions on Microwave Theory and Techniques*, vol. 63, no. 9, pp. 2730–2740, 2015.
[22] M. N. Akinci, M. Abbak, S. Özgür, M. Çayören, and I. Akduman, "Experimental comparison of qualitative inverse scattering methods," in *2014 IEEE Conference on Antenna Measurements & Applications (CAMA)*, 2014, pp. 1–4.
[23] M. N. Akinci, M. Çayören, and I. Akduman, "Near-field orthogonality sampling method for microwave imaging: Theory and experimental verification," *IEEE Transactions on Microwave Theory and Techniques*, vol. 64, no. 8, pp. 2489–2501, 2016.
[24] R. Fazli, M. Nakhkash, and A. A. Heidari, "Alleviating the practical restrictions for music algorithm in actual microwave imaging systems: Experimental assessment," *IEEE transactions on antennas and propagation*, vol. 62, no. 6, pp. 3108–3118, 2014.
[25] E. Bilgin, M. Çayören, S. Joof, G. Cansiz, T. Yilmaz, and I. Akduman, "Single-slice microwave imaging of breast cancer by reverse time migration," *Medical Physics*, vol. 49, no. 10, pp. 6599–6608, 2022.
[26] A. Abbosh, B. Mohammed, and K. Bialkowski, "Differential microwave imaging of the breast pair," *IEEE Antennas and Wireless Propagation Letters*, vol. 15, pp. 1434–1437, 2015.
[27] M. Safak Kaplan, "Machine learning based augmentation of medical microwave imaging,", Istanbul Technical University Graduate Program, 2022.
[28] M. Lazebnik, M. Okoniewski, J. H. Booske, and S. C. Hagness, "Highly accurate Debye models for normal and malignant breast tissue dielectric properties at microwave frequencies," *IEEE microwave and wireless components letters*, vol. 17, no. 12, pp. 822–824, 2007.
[29] C. Gabriel, "Tissue equivalent material for hand phantoms," *Physics in Medicine & Biology*, vol. 52, no. 14, p. 4205, 2007.
[30] M. Y. Kanda, M. Ballen, S. Salins, C.-K. Chou, and Q. Balzano, "Formulation and characterization of tissue equivalent liquids used for R F densitometry and dosimetry measurements," *IEEE Transactions on microwave theory and techniques*, vol. 52, no. 8, pp. 2046–2056, 2004.
[31] B. Saçlı, C. Aydınalp, G. Cansız, S. Joof, T. Yilmaz, M. Çayören, B. Önal, and I. Akduman, "Microwave dielectric property-based classification of renal calculi: Application of a knn algorithm," *Computers in biology and medicine*, vol. 112, p. 103366, 2019.
[32] U. B. Çalışkan, C. Aydınalp, and T. Y. Abdolsaheb, "Comparing two fitting algorithms to determine Cole-Cole parameters," in *2023 31st Signal Processing and Communications Applications Conference (SIU)*. IEEE, 2023, pp. 1–4.

BIOGRAPHIES

Cemanur Aydinalp received the B.S. degree from the Department of Electronics Engineering, Ankara University, Ankara, Turkey, in 2011. The M.S. degree from the Department of Electrical and Computer Engineering, San Diego State University, San Diego, USA, in 2015. She completed her Ph.D. degree in the Department of Telecommunication Engineering at Istanbul Technical University, Istanbul, Turkey. She is currently working as a research assistant at Istanbul Technical University. Her research interests include microwave dielectric spectroscopy, data analysis, optimization of open-ended coaxial probes, and application of supervised machine learning algorithms to engineering problems.

Gulsah Yildiz received the B.S. and M.Sc. degrees from the Department of Electrical and Electronics Engineering, İ.D. Bilkent University, Ankara, Turkey, in 2016 and 2018. She completed her Ph.D. degree in Telecommunication Engineering, Istanbul Technical University, Istanbul, Turkey. She is currently working as an assistant professor at Istanbul Technical University. Her research interests are microwave imaging, microwave hyperthermia, the application of deep learning, and physics-induced neural network algorithms to engineering problems.